Eddy current simulation in thick cylinders of finite length induced by coils of arbitrary geometry

Hector Sanchez Lopez *, Michael Poole, Stuart Crozier

The University of Queensland, School of Information Technology and Electrical Engineering, Qld 4072, Australia

ABSTRACT

Eddy currents are inevitably induced when time-varying magnetic field gradients interact with the metallic structures of a magnetic resonance imaging (MRI) scanner. The secondary magnetic field produced by this induced current degrades the spatial and temporal performance of the primary field generated by the gradient coils. Although this undesired effect can be minimized by using actively and/or passively shielded gradient coils and current pre-emphasis techniques, a residual eddy current still remains in the MRI scanner structure. Accurate simulation of these eddy currents is important in the successful design of gradient coils and magnet cryostat vessels. Efficient methods for simulating eddy currents are currently restricted to cylindrical-symmetry. The approach presented in this paper divides thick conducting cylinders into thin layers (thinner than the skin depth) and expresses the current density on each as a Fourier series. The coupling between each mode of the Fourier series with every other is modeled with an inductive network method. In this way, the eddy currents induced in realistic cryostat surfaces by coils of arbitrary geometry can be simulated. The new method was validated by simulating a canonical problem and comparing the results against a commercially available software package. An accurate skin depth of 2.76 mm was calculated in 6 min with the new method. The currents induced by an actively shielded *x*-gradient coil were simulated assuming a finite length cylindrical cryostat consisting of three different conducting materials. Details of the temporal–spatial induced current diffusion process were simulated through all cryostat layers, which could not be efficiently simulated with any other method. With this data, all quantities that depend on the current density, such as the secondary magnetic field, are simply evaluated.

© 2010 Elsevier Inc. All rights reserved.

1. Introduction

According to Faraday's law, voltage is induced in a conducting object when it is under the influence of a time-varying magnetic field. If a closed conducting path exists, then time-varying current flows in the conducting object; these are commonly referred as eddy currents. Eddy currents, like a current flowing in a wire, produce Ohmic heating, Lorentz forces (when immersed in an external magnetic field) and time-varying magnetic fields. Superconducting magnets for magnetic resonance imaging (MRI) scanners are usually contained in a multi-cylindrical conducting cryostat structure. The cryostat contains cryogens (e.g. liquid Helium) that maintain the superconducting properties of the magnet wires whilst also providing enough support to counteract the large magnetic forces and mechanical stresses. Magnetic field gradient coils are rapidly switched to encode the precessional frequency of the nuclear spin with spatial position by a linear variation of the axial magnetic field component along the *x*, *y* and *z* coordinates. As the gradient coils are switched, they invariably induce complex spatial and time-varying eddy currents within the conducting structure of the MRI scanner. These eddy currents in turn, generate a time-dependent magnetic field in the region of interest (ROI). This undesired *secondary* magnetic field opposes and distorts the linear *primary* gradient field generated by the gradient coils. This results in a miss-location of the NMR signal and consequential image distortion [1–3]. Aluminum cylinders cooled to 4K usually form part of the magnet support and cryostat. Hence, when gradient coils are switched, long-lasting eddy currents are induced in these structures [4–7] since their conductivity is high. The secondary fields can build up over time if the repetition time of gradient pulses is shorter than the longest eddy current decay constant. This undesired effect produces thermal load in the cryostat vessel which may lead to increased boil-off of the cryogens or even cause magnet quenching in extreme cases. Another undesired effect of the induced currents is acoustic noise due to their interaction with the B_0 field [8]. Although the many deleterious effects of eddy currents have been greatly reduced by using active and passive shielding coils [9–12], current pulse pre-emphasis [3], trials of less

* Corresponding author.
   E-mail addresses: hsanchez@itee.uq.edu.au (H. Sanchez Lopez), michael@itee.uq.edu.au (M. Poole), stuart@itee.uq.edu.au (S. Crozier).

conducting magnet bore material and cryostat configurations [6,7], residual and complex eddy currents remains a problem in MRI. Hence, an accurate numerical evaluation of these residual currents is of continued importance in MRI.

The large-scale calculation of eddy currents in conductors of complex geometry is computationally challenging, particularly, if the source of the field excitation has a 3D current distribution. For transient analysis, the problem becomes even more challenging to solve. A variety of differential and integral methods have been proposed to simulate the phenomena of eddy current induction in MRI. The finite element method (FEM) and finite difference time-domain (FDTD) schemes permit the simulation of realistic cryostat vessels and 3D gradient coils (x- and z-gradient coil) with large computational burden and some difficulties in the management of far field boundary conditions [7,13–15]. Field solutions are approximated at the origin in some differential schemes developed in cylindrical coordinates [15].

Integral methods, such as the boundary element method (BEM) [16], only require the discretization of the active parts, neglecting the surrounding air and introducing a correct far boundary condition. The BEM has some difficulty in simulating the thickness of the cryostat and its conducting properties. The equivalent magnetic coupling circuit (EMCC) or network method has been applied with some success in the analysis of currents induced by axis-symmetric coils (e.g. z-gradients) in a realistic cryostat [6,8,12]. To the knowledge of the authors, BEM analysis of an x-gradient coil or any other coil of arbitrary geometry has not been reported. The network method as an integral method [16,17], introduces a correct far boundary condition and allows a accurate simulation of the conducting domain.

This paper presents a network method coupled in Fourier space to accurately and efficiently evaluate the current induced by coils of arbitrary geometry in cylindrical coordinates. The new scheme combines the advantages of the differential and integral methods of including the physical properties of the model (cryostat thickness, length and conductivity) and a correct management of boundary conditions (magnetic field is accurately determined in the ROI without approximation). The three main assumptions of this new approach are: (a) an induced surface current density distribution is considered uniform across conducting cylindrical shells of thickness h; where h is much smaller than the skin depth for the given frequency, (b) the thickness h is much smaller that the cylinder axial length and radius, (c) no resistive coupling exists between shells but they are inductively coupled. Considering (a)–(c), we applied the infinitesimal thin shell approach where a surface current density, expressed as a finite Fourier series, flows in each cylindrical surface of radius ρ, conductivity σh and axial length L. Resistive losses and magnetic energy are rapidly calculated using Bessel functions [18], thereby avoiding costly full 3D computation of theses parameters in Cartesian coordinates. The accuracy and versatility of the method is demonstrated by modeling the induced current of an actively-shielded whole body x-gradient coil in a multi-layered cylindrical cryostat vessel. Details of the spatiotemporal current diffusion process within each layer and the magnetic field produced by each cylinder are presented and discussed.

2. Materials and methods

In this section the basic field equations and the assumptions under which the model is valid are presented. The diffusion equation, power dissipation, magnetic energy and the current density expression are described and presented for consistency of notation and completeness.

2.1. Basic equations and model assumptions

A non-magnetic metallic cylinder (region V_i) is immersed in an external magnetic field created by the known source $\mathbf{J}_s(\mathbf{r},t)$ excited at $t = 0$ (see Fig. 1). We assumed a linear isotropic conducting media of conductivity σ. The system is linear and the total contribution of magnetic field intensity can be represented by $\mathbf{H}_i(\mathbf{r},t) + \mathbf{H}(\mathbf{r},t)_s$; where $\mathbf{H}_s(\mathbf{r},t)$ is the magnetic field intensity produced by the known current source $\mathbf{J}_s(\mathbf{r},t)$ immersed in the medium of $\sigma = 0$ and $\mu_0 = 4\pi\,10^{-7}$ H/m. $\mathbf{H}_i(\mathbf{r},t)$ is the magnetic field generated by the induced currents in V_i. We assumed that currents and fields may change in both space and time.

It is assumed that no net electric charges exist and the displacement current caused by the change of polarization in the medium is much smaller than the conducting current $\mathbf{J}_i(\mathbf{r},t) = \sigma\,\mathbf{E}(\mathbf{r},t)$, where $\mathbf{E}$ is the electric field produced by $\mathbf{J}_i(\mathbf{r},t)$. The electromagnetic field equations in the presence of the conducting cylinder V_i are giving by:

$$\nabla \times (\mathbf{H}_i(\mathbf{r},t) + \mathbf{H}_s) = \begin{cases} \mathbf{J}_i(\mathbf{r},t) & \mathbf{r} \in V_i \\ \mathbf{J}_s(\mathbf{r},t) & \mathbf{r} \in \Re^3 | \mathbf{r} \notin V_i \end{cases} \quad (1)$$

$$\nabla \cdot (\mathbf{H}_i(\mathbf{r},t) + \mathbf{H}_s(\mathbf{r},t)) = 0 \qquad \mathbf{r} \in \Re^3 | \mathbf{r} \notin V_i \quad (2)$$

We assumed that the source $\mathbf{J}_s(\mathbf{r},t)$ is known and excited at $t = 0$, $\mathbf{J}_i$ and $\mathbf{H}_i$ are considered zero at $t = 0$ [19].

The conducting cylinder V_i is divided in N layers of thickness h, where h is much smaller than the skin depth for the given frequency. The shell axial length L and radius ρ_n are much larger than the thickness h. The conducting layers C_n are smooth and treated as thin shells of surface conductivity σh. We assumed that no current flows in the radial direction ($J_\rho \approx 0$), hence no resistive coupling exists between the shells, but that they are inductively coupled. In regards of the aforementioned conditions the current induced in the shell is treated as a surface current density and it is considered uniform across the sufficiently small thickness h. The induced current density has two components ($\mathbf{J}_i^s(\mathbf{r},t) = J_\phi(\mathbf{r},t)\mathbf{e}_\phi + J_z(\mathbf{r},t)\mathbf{e}_z$) and it is related to $\mathbf{J}_i(\mathbf{r},t)$ by $\mathbf{J}_i^s(\mathbf{r},t) = h\mathbf{J}_i(\mathbf{r},t)$. $J_\phi(\mathbf{r},t)$ and $J_z(\mathbf{r},t)$ are the azimuthal and axial components of the induced current in C_n, respectively. Under this assumptions $\mathbf{J}_i^s(\mathbf{r},t)$ can be expressed as
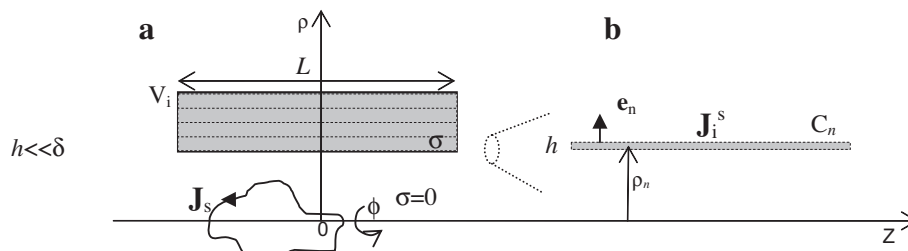
Fig. 1. Schematic representation of the model. (A) Half cross-section of the metallic cylinder of conductivity σ immersed in a magnetic field created by the known exciting source, $\mathbf{J}_s(\mathbf{r},t)$. The thickness h is much smaller than the skin depth, δ. (B) A surface current density $\mathbf{J}_i^s(\mathbf{r},t)$ flows in each thin conducting surface C_n of axial length L. The normal vector $\mathbf{e}_n$ points outward the surface of mean radius ρ_n.
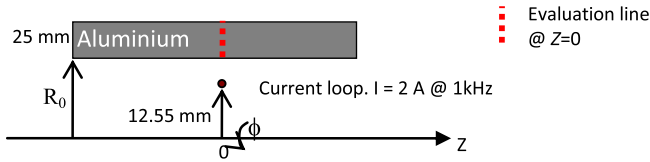
Fig. 2. Half cross-section of the conducting cylinder excited by a concentric circular current loop place at $z = 0$.

the rotor of the electric vector potential, **T**, of which, only one component exists which points normal to C_n. Then $\mathbf{J}_i^s$ is expressed as [20]:

$$\mathbf{J}_i^s = \nabla \times \psi(z, \phi, t)\mathbf{e}_n \qquad (3)$$

where $\psi(z, \phi, t)$ is the stream function. In virtue of the source-free condition $\nabla \cdot \mathbf{J}_i^s(\mathbf{r}, t) = 0$, both components of the vector $\mathbf{J}_i^s(\mathbf{r}, t)$ can be related such as $\nabla \cdot \mathbf{J}_i^s(\mathbf{r}, t) = 0$ holds.

It is assumed that the exciting source is represented by an infinitely thin wire filament of current density

$$\mathbf{J}_s(\mathbf{r}, t) = \sum_{j=1}^{H} s(t) \frac{\mathbf{l}_j(\mathbf{r})}{|\mathbf{l}_j(\mathbf{r})|} \qquad (4)$$

where $\mathbf{l}_j = (l_x\mathbf{e}_x + l_y\mathbf{e}_y + l_z\mathbf{e}_z)$ is the vector that joins two consecutive points of the discrete coil. We assumed that the points are sorted in such a way that vector $\mathbf{l}$ is directed to the current direction. H is the number of segments and

$$s_s(t) = I_0 I(t) \qquad (5)$$

is the time variation of the driving current applied to the exciting coil. I_0 is the current amplitude.

2.2. Current density

The induced current density components may contain all possible spatial variation along the ϕ- and z-directions in order to support exciting coils of an arbitrary geometry. Some of the approaches presented are suitable for coils of a specific geometry or for infinitely long cylinders [21,22]. In this paper we propose to express the azimuthal component of $\mathbf{J}_i^s(\mathbf{r},t)$ as normalized Fourier
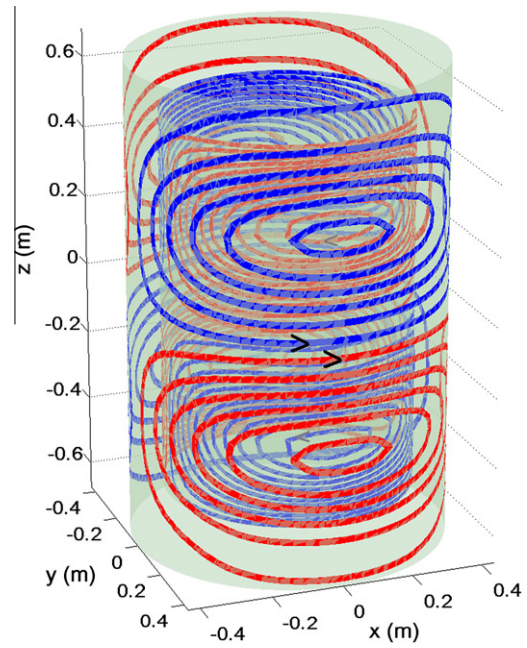
Fig. 4. A representation of the designed x-gradient coil. The arrows indicate the current direction.

series expressed as function of the coordinates (ϕ- and z-) and the variable time t; thus:

$$
J_\phi(z, \phi, \rho, t)
$$
$$
= \sum_{n=1}^{N} \delta(\rho - \rho_n) \cdot \left[\overbrace{\left[\sum_{q=0}^{Q-1} \beta_{nq}(t)\cos(K_q z) + \sum_{q=1}^{Q} \alpha_{nq}(t)\sin(K_q z) \right]}^{a} \lambda_0 \right.
$$
$$
\left. + \overbrace{\left[\sum_{q=1}^{Q} \theta_{nq}(t)\cos(K_q z) + \sum_{q=1}^{Q} \xi_{nq}(t)\sin(K_q z) \right]}^{b} \sum_{m=1}^{M} \lambda_m e^{im\phi} \right]
$$
$$(6)$$
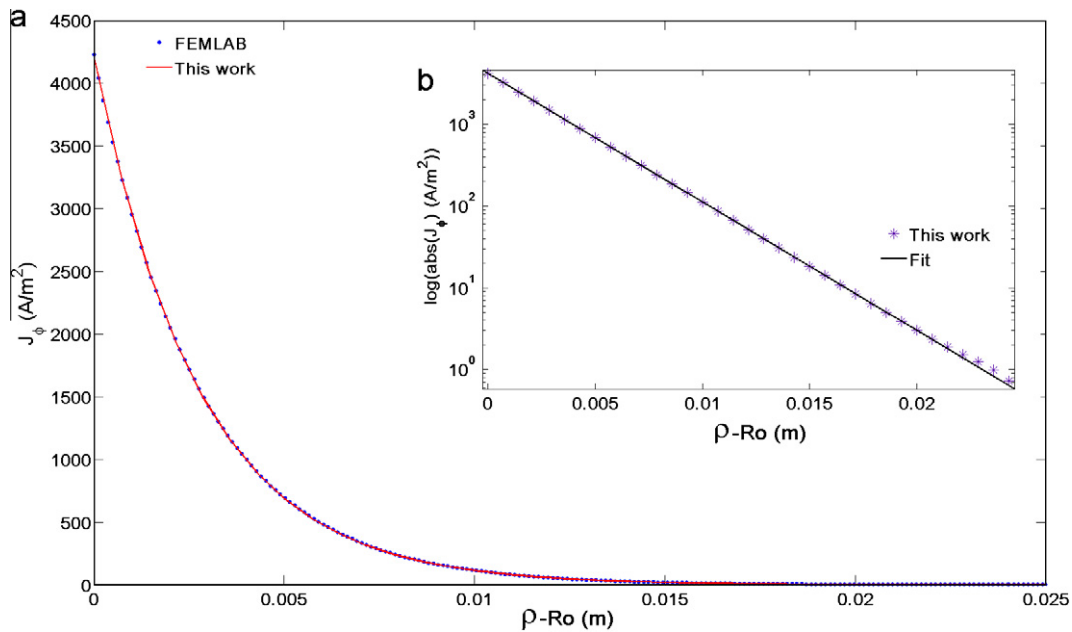
Fig. 3. (a) Eddy current penetration in a thick conducting cylinder versus radial distance at $z = 0$. The cylinder is excited by a loop driven with a time-harmonic current variation. (b) The new approach presented in this paper is compared with a single exponential fitting $y(\rho) = 4180e^{-362.2(\rho - Ro)}$. The solution obtained with this work indicates the accuracy of the method.

where the functions *cos* and *sin* represents the basis function and $\beta_{nq}(t)$, $\alpha_{nq}(t)$, $\theta_{nq}(t)$ and $\xi_{nq}(t)$ are the unknown amplitude of the current modes expressed as a function of time. Q is the number of basis functions, λ_0 and λ_m are weighting factors; and $K_q = \frac{2\pi q}{L}$. $\mathbf{J}_i^s(\mathbf{r},t) = 0$ for $|z| > L/2$. The proposed current density component includes the cylinder length [23].

The term **a** in Eq. (6) includes all even and odd dependence of $\mathbf{J}_i^s$ along z-direction ($m = 0$); including the constant term $\beta_{n0}(t)$ useful to quantify the B_0 shift due to the eddy currents [24]. If only coils with $J_z(\mathbf{r},t) = 0$ are used as exciting coils, then the term **b** might be excluded. However, when analyzing coils with $J_z(\mathbf{r},t)$ dependence ($m \neq 0$), then the terms **a** and **b** with $m = 1,2,\ldots,M$ must be included. When evaluating the induced current by an x-gradient coil, then only $m = 1$ terms are included. It is required to incorporate high order terms ($M > 1$) when complicated 3D coil current patterns are used as exciting coils.

When evaluating Eq. (6) the weighting factors λ_0 and λ_m are equal to one; the uses of these parameters are explained in the next section.

2.3. Diffusion equation, power and magnetic energy

The diffusion equation is deduced using the law of conservation of energy and can be written as [19,25]:

$$\mathbf{M}_{is}\left(\frac{\partial \mathbf{J}_s(t)}{\partial t}\right) + \mathbf{M}_{ii}\left(\frac{\partial \mathbf{J}_i^s(t)}{\partial t}\right) + \mathbf{R}_{ii}\left(\mathbf{J}_i^s(t)\right) = 0. \tag{7}$$

This equation relates the induced current with the exciting current source. $\mathbf{M}_{is}$ is the mutual inductive coupling between the source and the conducting shells, $\mathbf{M}_{ii}$ and $\mathbf{R}_{ii}$ are the self inductive and resistive coupling of the conducting shells, respectively.
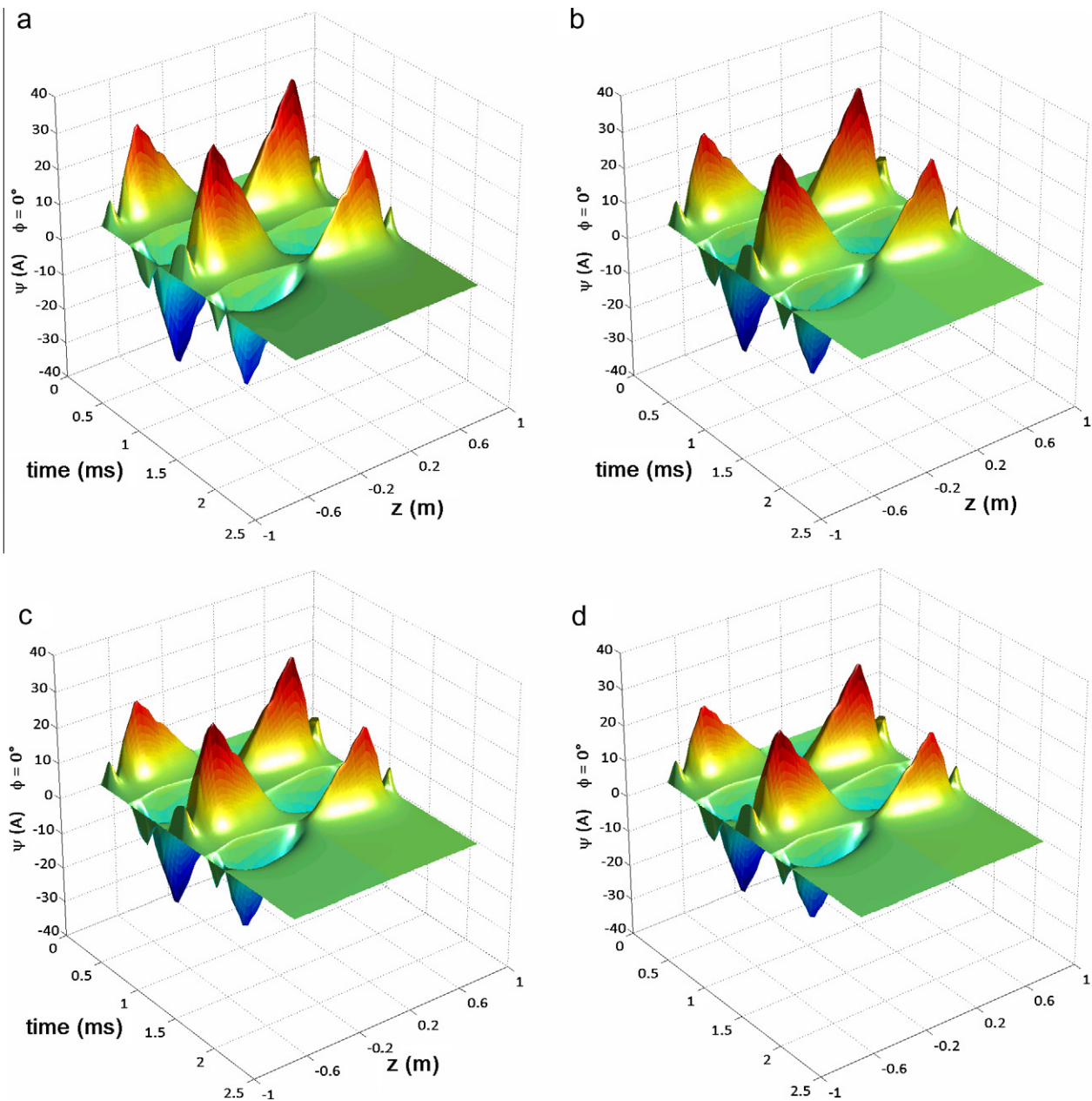
Fig. 5. Stream function of the currents induced by a shielded x-gradient coil as function of z and time. Layers 1(a), 2(b), 3(c) and 4(d) belonging to the warm bore cylinder.

One of the advantages of using Fourier Bessel expression is that the self resistance and inductance depends on the Fourier transform of the azimuthal current density and only a single integral over k is required. Appendix A and B details the power dissipated and the magnetic energy expressions deduced from Eqs. (33 and 34) (page 912) [18]. The Fourier transform of Eq. (6) results in [26,27]:

$$j_\phi^m(\rho, k) = \sum_{n=1}^{N} \delta(\rho - \rho_n) \left\{ \overbrace{\lambda_0 \left(\sum_{q=0}^{Q-1} \beta_{nq}(t) g_q^+(k, L) + i \sum_{q=1}^{Q} \alpha_{nq}(t) g_q^-(k, L) \right)}^{a} \atop \underbrace{\lambda_m \left(\sum_{q=1}^{Q} \theta_{nq}(t) g_q^+(k, L) + i \sum_{q=1}^{Q} \xi_{nq}(t) g_q^-(k, L) \right)}_{b} \right\}.$$

(8)

From references [26,27] we deduced that:

$$g_q^\pm(k, L) = \frac{L}{2} \left(\mathrm{sinc}\left(\frac{kL}{2} + q\pi \right) \pm \mathrm{sinc}\left(\frac{kL}{2} - q\pi \right) \right).$$

(9)

The superscript $\pm$ in Eq. (6) is used to identify the spatial dependence of the basis; for cos (symmetry in z-axis) function we used (+) and for sin (anti-symmetry) we used (−).

The mutual coupling ($\mathbf{M}_{is}$) between an arbitrary exciting coil described by $\mathbf{J}_s(t)$ and the conducting shells C_n is calculated in the real space. The currents induced by asymmetric [28], locals [29], uniplanar [30] and 3D [31] gradient coils excited by arbitrary current pulse can be evaluated. The mutual coupling formula for coils with symmetric current density along z-axis and zero axial component is written as:

$$M_{is}^{0+} = \frac{\mu_0}{4\pi} \sum_{n=1}^{N} \sum_{q=0}^{Q-1} \beta_{nq}(t) M_{nq}^{0+}$$

(10)
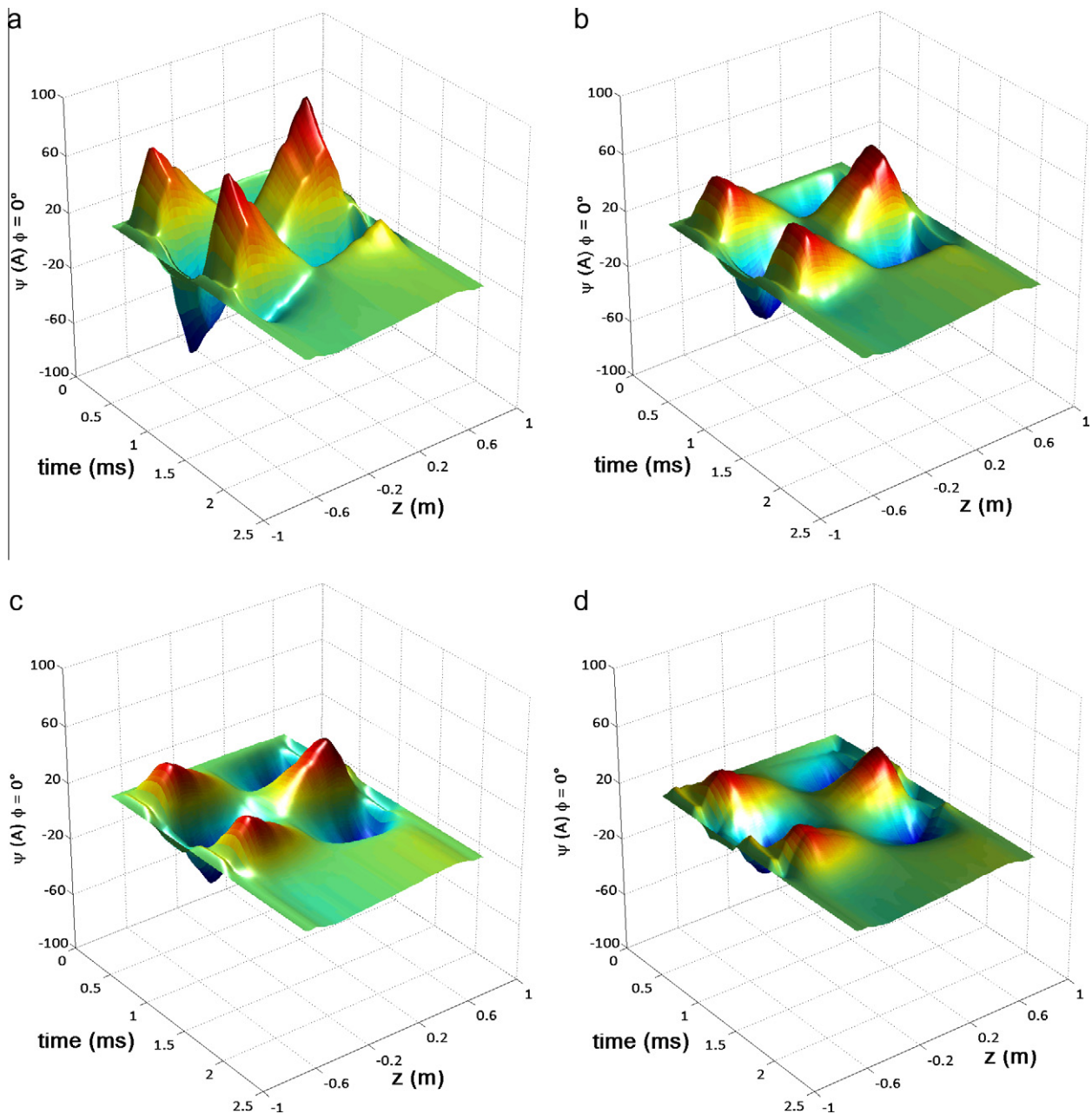
Fig. 6. Stream function of the currents induced by a shielded x-gradient coil as function of z and time. Layers 1(a), 2(b), 3(c) and 4(d) belonging to the 80 K cylinder.

where

$$M_{nq}^{0+} = \int_{-L/2}^{L/2} \int_0^{2\pi} \frac{\sum_{j=1}^H \left(-l_{x_j}\sin(\phi') + l_{y_j}\cos(\phi')\right)\rho_n \cos(K_{nq}z')d\phi'dz'}{\upsilon_{jn}}. \tag{11}$$

Eq. (10) is deduced by substituting Eqs. (4) and (6) in the stored magnetic energy formula (page 147. Eq. (3.63)) [32].

$\upsilon_{jn} = \sqrt{(r_{x_j} - \rho_n \cos(\phi'))^2 + (r_{y_j} - \rho_n \sin(\phi'))^2 + (r_{y_j} - z')^2}$ is the distance between the discrete coil segments at the position (r_{xj}, r_{yj}, r_{zj}) and the differential element of area $\rho_n d\phi' dz'$. For cases where $J_\phi(\mathbf{r},t)$ is anti-symmetric along the z-axis and $J_z(\mathbf{r},t) = 0$, we have:

$$M_{is}^{0-} = \frac{\mu_0}{4\pi} \sum_{n=1}^N \sum_{q=1}^Q \alpha_{nq}(t) M_{nq}^{0-} \tag{12}$$

$$M_{nq}^{0-} = \int_{-L/2}^{L/2} \int_0^{2\pi} \frac{\sum_{j=1}^H \left(-l_{x_j}\sin(\phi') + l_{yj}\cos(\phi')\right)\rho_n \sin(K_{nq}z')d\phi'dz'}{\upsilon_{jn}}. \tag{13}$$

For cases $m \neq 0$ and symmetric variations of $J_\phi(\mathbf{r},t)$ along z- and ϕ-directions the mutual coupling results:

$$M_{is}^{m+} = \frac{\mu_0}{4\pi} \sum_{n=1}^N \sum_{q=1}^Q \theta_{nq}(t) M_{nq}^{m+} \tag{14}$$

where

$$M_{nq}^{m+} = \int_{-L/2}^{L/2} \int_0^{2\pi} \sum_{j=1}^H \frac{\rho_n}{\upsilon_{jn}} \left\{ \begin{array}{l} \left(-l_{x_j}\sin(\phi') + l_{y_j}\cos(\phi')\right) \\ \times \cos(K_{nq}z')\cos(m\phi') \\ +l_{z_j}J_z^{m+}(z',\phi',\rho_n)\sin(m\phi') \end{array} \right\} d\phi'dz', \tag{15}$$

and for anti-symmetric variations $J_\phi(\mathbf{r},t)$ along the z-axis the mutual coupling is written as:

$$M_{is}^{m-} = \frac{\mu_0}{4\pi} \sum_{n=1}^N \sum_{q=1}^Q \xi_{nq}(t) M_{nq}^{m-} \tag{16}$$

where

$$M_{nq}^{m-} = \int_{-L/2}^{L/2} \int_0^{2\pi} \sum_{j=1}^H \frac{\rho_n}{\upsilon_{jn}} \left\{ \begin{array}{l} \left(-l_{x_j}\sin(\phi') + l_{y_j}\cos(\phi')\right) \\ \times \sin(K_{nq}z')\cos(m\phi') \\ +l_{z_j}J_z^{m-}(z',\phi',\rho_n)\sin(m\phi') \end{array} \right\} d\phi'dz'. \tag{17}$$

Similar expressions to Eqs. (15) and (17) can be simply deduced for anti-symmetric variations along ϕ. Expression for the axial component of induced current density $J_z^{m\pm}$ can be found from the condition $\nabla \cdot \mathbf{J}_i^s = 0$.

Substituting Eqs. (A.2), (A.3), (A.5), (A.6), (B.2), (B.3), (B.5) and (B.6) and Eqs. (11), (13), (15) and (17) in Eq. (7), the diffusion equation results:

$$\overbrace{\begin{pmatrix} L_{nq,n'q'}^{0+} & 0 & 0 & 0 & 0 & 0 & 0 \\ 0 & L_{nq,n'q'}^{0-} & 0 & 0 & 0 & 0 & 0 \\ 0 & 0 & L_{nq,n'q'}^{m+} & 0 & 0 & 0 & 0 \\ 0 & 0 & 0 & L_{nq,n'q'}^{m-} & 0 & 0 & 0 \\ 0 & 0 & 0 & 0 & \dots & 0 & 0 \\ 0 & 0 & 0 & 0 & 0 & L_{nq,n'q'}^{M+} & 0 \\ 0 & 0 & 0 & 0 & 0 & 0 & L_{nq,n'q'}^{M-} \end{pmatrix}}^{\mathbf{M}_{ii}} \frac{d\mathbf{s}_i}{dt}$$

$$+ \cdots \overbrace{\begin{pmatrix} P_{nq,n'q'}^{0+} & 0 & 0 & 0 & 0 & 0 & 0 \\ 0 & P_{nq,n'q'}^{0-} & 0 & 0 & 0 & 0 & 0 \\ 0 & 0 & P_{nq,n'q'}^{m+} & 0 & 0 & 0 & 0 \\ 0 & 0 & 0 & P_{nq,n'q'}^{m-} & 0 & 0 & 0 \\ 0 & 0 & 0 & 0 & \dots & 0 & 0 \\ 0 & 0 & 0 & 0 & 0 & P_{nq,n'q'}^{M+} & 0 \\ 0 & 0 & 0 & 0 & 0 & 0 & P_{nq,n'q'}^{M-} \end{pmatrix}}^{\mathbf{R}_{ii}} \mathbf{s}_i$$

$$= - \overbrace{\begin{pmatrix} M_{nq}^{0+} \\ M_{nq}^{0-} \\ M_{nq}^{m+} \\ M_{nq}^{m-} \\ \dots \\ M_{nq}^{M+} \\ M_{nq}^{M-} \end{pmatrix}}^{\mathbf{M}_{is}} \frac{ds_s(t)}{dt} \tag{18}$$

where $\mathbf{s}_i(t) = (\beta_{nq}^0(t), \alpha_{nq}^0(t), \theta_{nq}^m(t), \xi_{nq}^m(t), \dots, \theta_{nq}^M(t), \xi_{nq}^M(t))$ is the vector that contains the unknown amplitudes of the Fourier modes representing the induced current.

2.4. The time-harmonic and transient solution

For the time-harmonic analysis, $I(t)=e^{i\omega t}$ in Eq. (5) and the solution of Eq. (18) can be expressed as:

$$\mathbf{s}_i(\omega) = -i\omega(i\omega\mathbf{M}_{ii} + \mathbf{R}_{ii})^{-1}\mathbf{M}_{is} \tag{19}$$

for a given frequency ω.

Continuous function might be assigned to $I(t)$ when transient solutions are required. Specifically, we combined a set of membership fuzzy functions [33] to create sequences of current pulses.

Eq. (18) can be solved and expressed as function of the natural eigenmodes and eigenvalues of the conducting cylinder V_i [19,34]. We used the Crank Nicholson time stepping procedure to solve Eq. (18); however the (Galerkin and Euler) methods can be simply implemented by changing a constant value in the formulation [35].

In MRI we are usually interested in the axial component of the magnetic field (B_z). The field contribution in the ROI produced by $\mathbf{J}_i^s$ in each shell can be determined using the Biot–Savart law in real space, once the vector $\mathbf{s}_i$ is calculated. Other magnitudes such as induced force and torque are calculated using the full description of the induced current density $\mathbf{J}_i^s$.

The new eddy current calculation method was implemented in Matlab [33] using a XEON 2.5 GHz/32GB RAM computer server platform.

2.5. Validation of the computational method

The method was validated against commercial software FEM-LAB using a canonical problem. The problem consisted in predicting the skin depth of a current induced by a single loop in a finite length thick conducting cylinder. We considered a single filamentary circular current loop placed at the center of a conducting cylinder of axial length 38.6 cm, thickness 2.5 cm and internal radius R_0 = 17.5 cm. The cylinder conductivity at room temperature was set to σ = 32.26 × 10^6 S/m and we assumed that the current loop is driven by a harmonically varying current $I(t) = e^{i\omega t}$ with an amplitude I_0 = 2 A, $\omega = 2\pi \times$ f and f = 1 kHz. The loop of radius 12.55 cm was placed concentrically with respect to the cylinder axial axis and at z = 0. Fig. 2 shows a 2D representation of the described example.

The cylinder was divided in to 35 layers and the time-harmonic solution Eq. (19) was applied. This model only required the calculation of the matrices $L_{nq,n'q'}^{0\pm}$ (Eqs. (A.5) and (A.6)), $P_{nq,n'q'}^{0\pm}$

(Eqs. (A.2) and (A.3)) and the vectors $M_{nq}^{0\pm}$ to obtain the amplitude $\mathbf{s}_i(\omega) = (\beta_{nq}^0(\omega)$ and $\alpha_{nq}^0(\omega))$ of the induced current $\mathbf{J}_i^s$.

An equivalent model was setup in FEMLAB. A coil of finite circular cross-section was placed in the same position of the current loop model. The radius of the circular cross-section was set to 1 mm to simulate a filamentary loop. This value produces a current density of 636.62 × 10^3 A/m². The model domain was discretized using 19401 triangular elements to obtain 35 layers along the radial directions.

3. Results

3.1. Validation

Fig. 3 shows the results produced by the presented method (This work) and the result obtained using FEMLAB.

FEMLAB takes advantage of the problem symmetry and the solution was obtained in 35 s. The solution produced with the
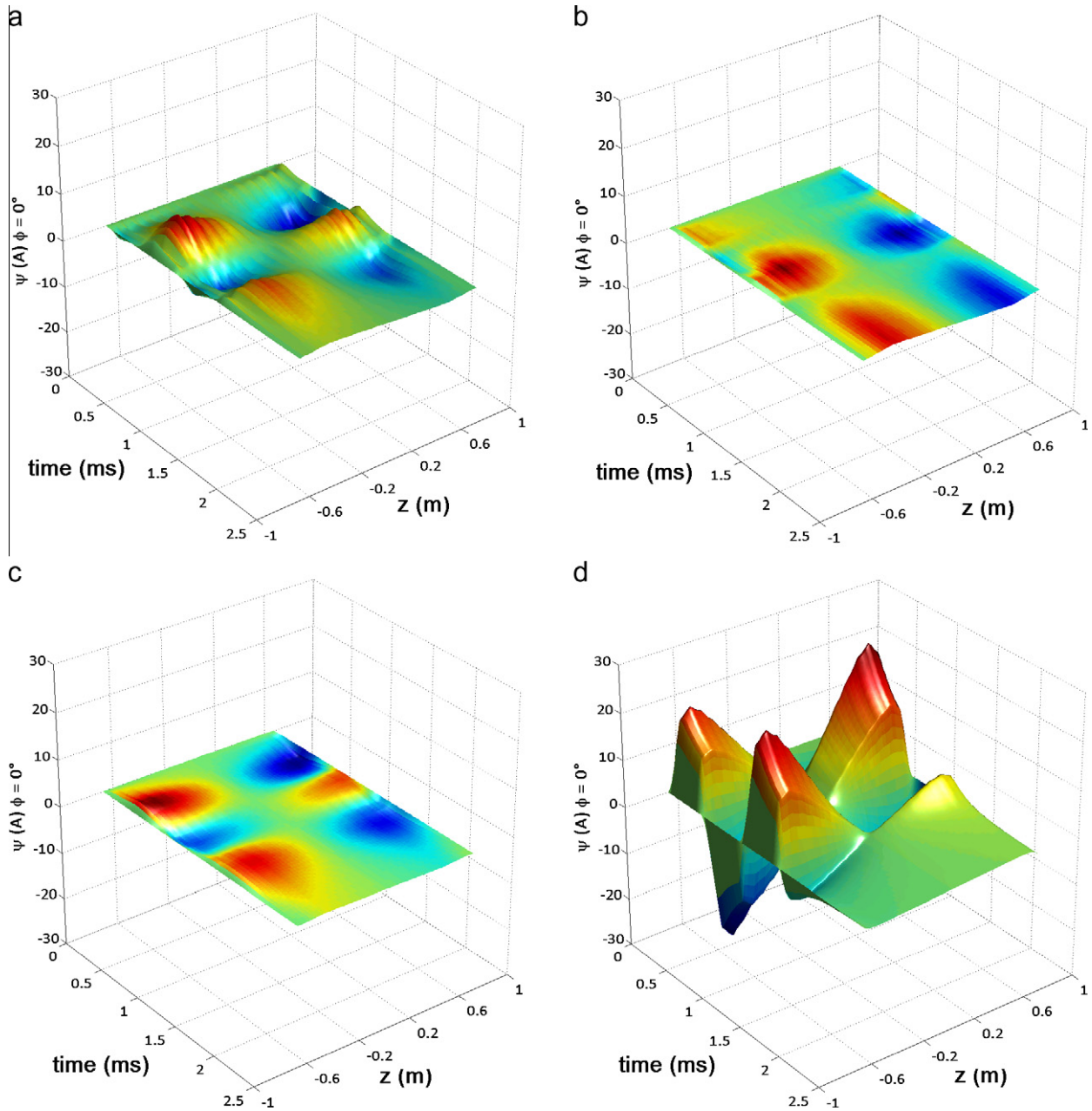
Fig. 7. Stream function of the currents induced by a shielded x-gradient coil as function of z and time. Layers 1(a), 4(b), 6(c) and 9(d) belonging to the 4 K cylinder.

new approach required 6 min to be completed. The root means square error of the curve fitting presented in Fig. 3b was 0.0997 and the r-square was 1. The skin depth penetration predicted by this work was 2.76 mm which is close to the 2.8 mm value predicted by the formula $\delta = \sqrt{\frac{2}{\sigma\mu_0\omega}}$.

3.2. Current induced by an actively-shielded whole body x-gradient coil

The main goal of presenting this example was to demonstrate the versatility of the method to deal with coil geometry that produces a 3D magnetic field such as x-gradient coils. Results detailing the current diffusion process through the thickness of the cylinders, as well as the magnetic field produced by each layer are presented.

The cryostat model consisted of three cylinders of axial length 1.4 m, 1.37 m and 1.35 m and thickness 5 mm, 3 mm and 6 mm, respectively. In cylinder 1 (warm shield) the radius was set to 45 cm, cylinder 2 (80 K radiation shield) the radius was 46.5 cm and cylinder 3 (4 K radiation shield) the radius was set to 47.8 cm.

The conductivity of each cylinder was set to 1.05×10^6 S/m (room temperature), 100×10^6 S/m (80 K) and 500×10^6 S/m (4 K) [36]. Fig. 4 shows an x-gradient coil designed using the equivalent magnetization current method [29].

The magnetic field produced in the surface of the second cylinder (80 K shield) was constrained to values smaller than 10 μT. The self inductance of this 18 turns per quarter coil was 196 μH and the efficiency η was 47.4 mT/m A. The gradient strength at the ROI was 21.3 mT/m. Assuming $I_0 = 450$ A, $I(t)$ was a sequence of three trapezoidal pulses with ramp up and ramp down times of 100 μs and
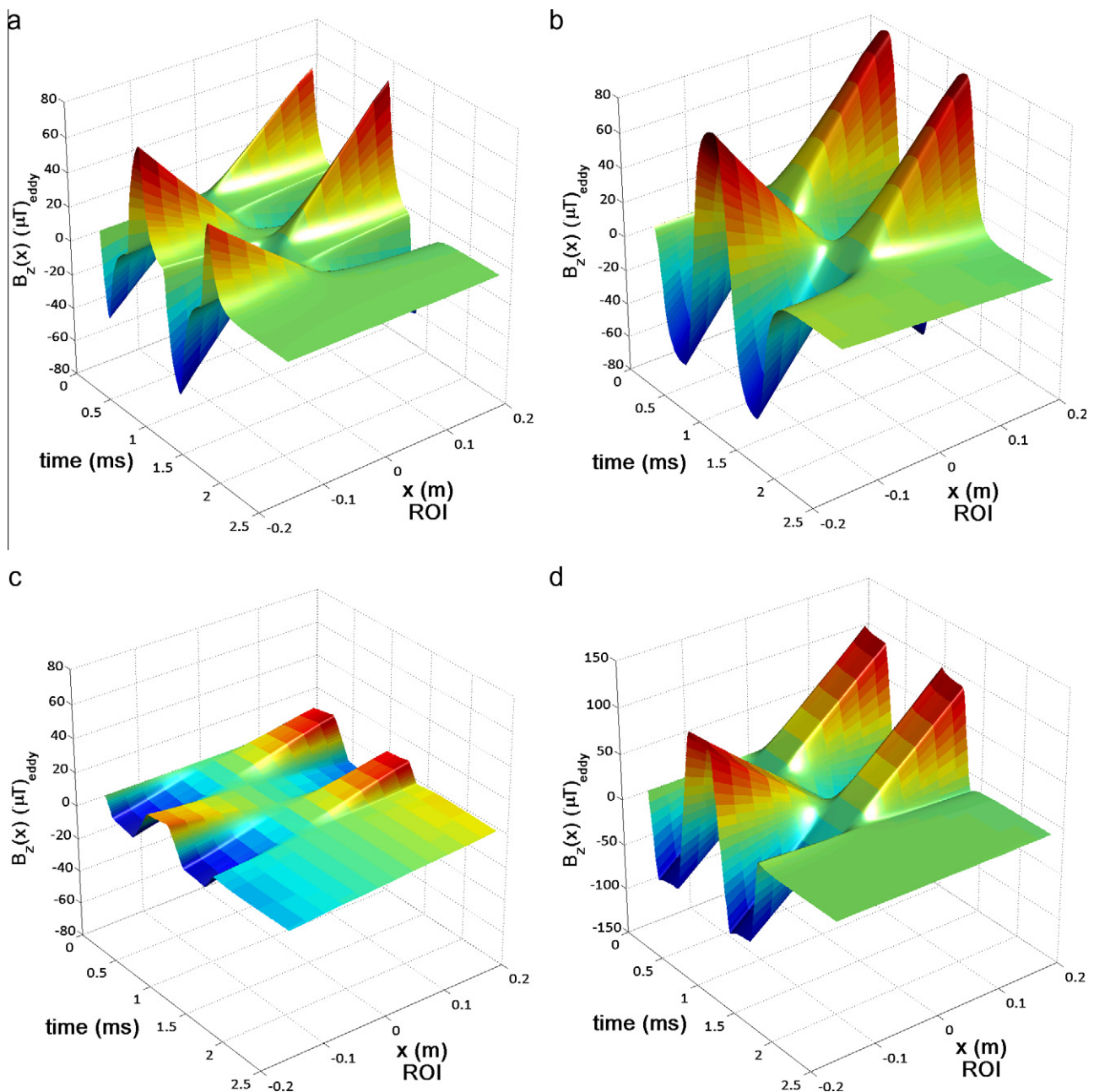
Fig. 8. Secondary magnetic field generated by the warm bore: (a) 80 K cylinder (b) (46.5 cm) and (c) 4 K cylinder (47.8 cm). (d) Transient analysis of the total magnetic field along the x-axis. The total magnetic field includes the contribution of the fields produced by the warm cylinder, 80 K and 4 K radiation shields, respectively.

flat-top of 300 μs. The time step was set to Δt = 10.05 μs to avoid possible oscillations of the Crank Nicholson method [35]. The warm and 80 K cylinders were divided in 4 layers each. The 4 K cylinder was divided in 9 layers to assure that the thickness, h, is smaller than the skin depth δ. The number of modes Q was set to 10 and M was set to 1. Fig. 5 shows the temporal behavior of the stream function along the axial direction in layers 1(a), 2(b), 3(c) and 4(d) belonging to the warm bore cylinder.

Fig. 6 shows the simulated eddy currents induced in the 80 K cylinder as function of time and z-position. Approximately 8000 wire segments were used to simulate the discrete x-gradient coil showed in Fig. 4.

Fig. 7 describes the transient analysis of four of the nine layers on which the 4 K cylinder was divided. Fig. 8 shows the transient of the secondary magnetic field contribution of all cylinders along the x-axis.

In virtue of the inclusion of the term **a** in Eq. (6), it was possible to evaluate the secondary magnetic field contribution produced by currents with m = 0 dependence. The first term **a** in Eq. (6) represents even variations of the current density along the z-axis including a constant value. This induced constant value $\beta_{n0}(t)$ produced an undesired offset in the resonant frequency of the tissue, leading to miss-registration of the spatial position of the sample [24]. Fig. 9 presents the B_0-shift induced by the x-gradient coil in the model cryostat.

The required computing time to complete the simulation was 25 min. FEM codes would require a huge computational burden [37] to simulate coils with 3D magnetic field such the coil evaluated in this work.

4. Discussion

4.1. Validation of the computational method

Fig. 3 demonstrates the accuracy of the new method when predicting the skin depth of the currents induced by a circular loop with a time-harmonic current variation. The predicted skin depth 2.76 mm is close to the target 2.8 mm yielded by the formula $\delta = \sqrt{\frac{2}{\sigma \mu_0 \omega}}$. An extremely small deviation of the simulated current with respect to the exponential fit for the outer shells was observed. We presume that this effect is due to the weak mutual

coupling between the source and the outer layers. The current tends to slightly increase its value as a compensating mechanism of the far-inductive coupling. A similar effect was observed in the results obtained from FEMLAB simulations and in Ref. [12].

The computing time required to complete the eddy current simulation strongly depends on the number of segments used to simulate the discrete coil. The Bessel functions are efficiently calculated in Matlab so that, for a typical model such as the ones presented in this paper (3 thick cylinders, 17 layers and Q = 10) the self inductive and resistance matrices are calculated in 8 min. However, the time required to calculate the mutual coupling Eq. (11), (13), (15) and (17) was approximately 16 min. This computing time can be reduced by using less numbers of wire segments H, at the expenses of accuracy.

4.2. Current Induced by an actively shielded body x-gradient coil

The thin shell approach allows us to express the induced current using the stream function ψ and hence the physical and mechanical magnitude that depends on $\mathbf{J}_i^s$ can be simply evaluated. Fig. 5 shows the stream function of the current induced in the layers belonging to the warm bore cylinder. Approximately 34 Å is the maximal peak current induced in the inner layer. ψ tends to decrease to 27 Å as the layer radius increases. In the warm bore cylinder 1, the current is rapidly dissipated as a typical response of materials with low conductivity. Eddy currents lasted considerably longer in the 80 K radiation shield cylinder, Fig. 6. This cylinder is usually in contact with liquid nitrogen and consequently possesses a higher conductivity. In virtue of the increased conductivity, the maximal peak stream function of the eddy current in the first layer was twice as large as that induced in the warm bore. However, the ψ maximal value rapidly decays when the cylinder radius increases. Conversely, the current remains almost constant through the thickness of the warm bore cylinder.

The 80 K radiation shield substantially reduces the peak of ψ to 6.5 Å in the first layers of the 4 K cylinder. (see Fig. 7a). The induced current has a very small value in layer 5 and tended to increase its value up to layer 9. The peak current of layer 9 of the 4 K cylinder is similar to the value generated in layer 1 of the warm bore cylinder. However, layer 9 is further from the ROI than layer 1 of the warm bore. Due to rapid current dissipation in the warm bore cylinder, the outer layers in the 4 K cylinder and the layers in the 80 K cylinder produces a significant contribution to the magnetic field (see Fig. 8d). In terms of amplitude, the warm and the 80 K cylinders (Fig. 8a and b) produce approximately the same peak magnetic field in the ROI. However, as mentioned before, the contribution from the warm cylinder dissipates quickly.

Fig. 9 presents the transient magnetic field contribution in the ROI along the z axis. Conversely to Fig. 8d, the B_0-shift effect is quickly dissipated in time even in the 80 K and 4 K radiation shield.

5. Conclusions

A new method to simulate the current induced by coils of arbitrary geometry in thick cylinders of finite length has been presented. The method combines the advantage of integral and differential schemes by correctly introducing far boundary conditions and physical properties to the model. The current induced in multiple thin layers was modeled as a truncated Fourier series expansion. The diffusion equation is then solved using the equivalent circuit network method. We have demonstrated that under the stated assumptions presented in the paper, the new method is able to accurately predict the skin depth in thick cylinders excited by coils of arbitrary geometry. The computational burden is substantially reduced by expressing the power and magnetic energy
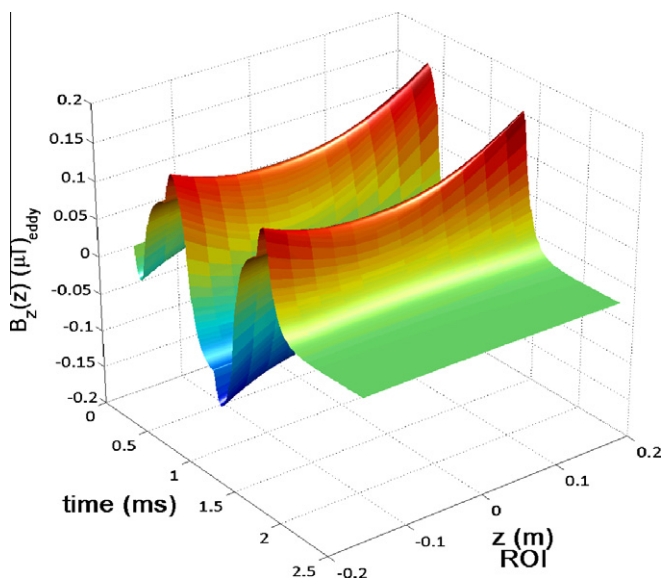
Fig. 9. Transient secondary magnetic field B_0-shift produced by the eddy currents induced in the cryostats.

matrices with a Fourier Bessel expansion. The presented formulation of the inductive coupling between the source and the conducting material permits the evaluation of coil of arbitrary geometry. A detailed study of the current diffusion process through thick cylinders is possible thanks to the use of the thin shell approach. Magnetic and electric fields, force, torque, mechanical vibration and acoustic noise analysis can be simulated in detail by using the presented approach. The analysis of the x-gradient coil showed that an increment of the induced current density was registered in the outer layers of the 4 K cylinder. This effect deserves a further analysis in terms of vibration and heating.

Acknowledgment

Appendix A. Case $m = 0$

From (Eqs. (33 and 34) page 912) [18] and Eq. (8) we write:

$$P^0 = \sum_{n=1}^{N} \sum_{n'=1}^{N} \left\{ \begin{array}{l} \sum_{q=0}^{Q-1} \sum_{q'=0}^{Q-1} \beta_{nq}^0(t)\beta_{n'q'}^0(t)P_{nq,n'q'}^{0+} \\ + \sum_{q=1}^{Q} \sum_{q'=1}^{Q} \alpha_{nq}^0(t)\alpha_{n'q'}^0(t)P_{nq,n'q'}^{0-} \end{array} \right\} \qquad (A.1)$$

where

$$P_{nq,n'q'}^{0+} = \frac{1}{\sigma h}\lambda_0 \int_{-\infty}^{\infty} dk \rho_n g_q^+(k,L)g_{q'}^+(k,L) \qquad (A.2)$$

$$P_{nq,n'q'}^{0-} = \frac{1}{\sigma h}\lambda_0 \int_{-\infty}^{\infty} dk \rho_n g_q^-(k,L)g_{q'}^-(k,L) \qquad (A.3)$$

for cases where the current density in the exciting coil is symmetric along z-axis and the axial components is. The magnetic energy is expressed as:

$$E^0 = \frac{1}{2}\sum_{n=1}^{N}\sum_{n'=1}^{N}\left\{ \begin{array}{l} \sum_{q=0}^{Q-1}\sum_{q'=0}^{Q-1}\beta_{nq}^0(t)\beta_{n'q'}^0(t)L_{nq,n'q'}^{0+} \\ + \sum_{q=1}^{Q}\sum_{q'=1}^{Q}\alpha_{nq}^0(t)\alpha_{n'q'}^0(t)L_{nq,n'q'}^{0-} \end{array}\right\} \qquad (A.4)$$

where

$$L_{nq,n'q'}^{0+} = -\mu_0 \int_{-\infty}^{\infty} dk \rho_n \rho_{n'} g_q^+(k,L)g_{q'}^+(k,L)I_0'(|k|\rho_n^<)K_0'(|k|\rho_{n'}^>). \qquad (A.5)$$

and

$$L_{nq,n'q'}^{0-} = -\mu_0 \int_{-\infty}^{\infty} dk \rho_n \rho_{n'} g_q^-(k,L)g_{q'}^-(k,L)I_0'(|k|\rho_n^<)K_0'(|k|\rho_{n'}^>). \qquad (A.6)$$

Eqs. (A.5) and (A.6) contain only the coupling between layers of small radius with layers of larger radius. The second half of the matrix is populated by symmetry in virtue that $L_{nq,n'q'}^{0\pm}$ and $P_{nq,n'q'}^{0\pm}$ are positive-definite and symmetric. The weighting factor $\lambda_0 = 1$.

Appendix B. Case $m \neq 0$

For cases when $m \neq 0$, the power matrix is written as:

$$P^m = \sum_{n=1}^{N}\sum_{n'=1}^{N}\left\{ \begin{array}{l} \sum_{q=1}^{Q}\sum_{q'=1}^{Q}\theta_{nq}^m(t)\theta_{n'q'}^m(t)P_{nq,n'q'}^{m+} \\ + \sum_{q=1}^{Q}\sum_{q'=1}^{Q}\xi_{nq}^m(t)\xi_{n'q'}^m(t)P_{nq,n'q'}^{m-} \end{array}\right\} \qquad (B.1)$$

where

$$P_{nq,n'q'}^{m+} = \frac{1}{\sigma h}\lambda_m \int_{-\infty}^{\infty} dk \rho_n g_q^+(k,L)g_{q'}^+(k,L)\left(1 + \frac{m^2}{k^2 \rho_n^2}\right), \qquad (B.2)$$

and

$$P_{nq,n'q'}^{m-} = \frac{1}{\sigma h}\lambda_m \int_{-\infty}^{\infty} dk \rho_n g_q^-(k,L)g_{q'}^-(k,L)\left(1 + \frac{m^2}{k^2 \rho_n^2}\right). \qquad (B.3)$$

The energy matrix is expressed as:

$$E^m = \frac{1}{2}\sum_{n=1}^{N}\sum_{n'=1}^{N}\left\{ \begin{array}{l} \sum_{q=1}^{Q}\sum_{q'=1}^{Q}\theta_{nq}^m(t)\theta_{n'q'}^m(t)L_{nq,n'q'}^{m+} \\ + \sum_{q=1}^{Q}\sum_{q'=1}^{Q}\xi_{nq}^m(t)\xi_{n'q'}^m(t)L_{nq,n'q'}^{m-} \end{array}\right\} \qquad (B.4)$$

where

$$L_{nq,n'q'}^{m+} = -\mu_0\lambda_m \int_{-\infty}^{\infty} dk \rho_n \rho_{n'} g_q^+(k,L)g_{q'}^+(k,L)I_m'(|k|\rho_n^<)K_m'(|k|\rho_{n'}^>) \qquad (B.5)$$

and

$$L_{nq,n'q'}^{m-} = -\mu_0\lambda_m \int_{-\infty}^{\infty} dk \rho_n \rho_{n'} g_q^-(k,L)g_{q'}^-(k,L)I_m'(|k|\rho_n^<)K_m'(|k|\rho_{n'}^>). \qquad (B.6)$$

For this case ($m \neq 0$) the parameter $\lambda_m = (2 - \delta_{m,0})$. Equations (B.5) and (B.6)) include only the interaction between layers of smaller radius with layers of larger radius. The second half of the matrix is populated by symmetry. The power matrices Eqs. (A.2), (A.3), (B.2) and (B.3) only include the coupling among Fourier modes belonging to the shell of radius ρ; there is no mutual resistive coupling between shells.

References

[1] C. Boesch, R. Gruetter, E. Martin, Temporal and spatial analysis of fields generated by eddy currents in superconducting magnets: optimization of corrections and quantitative characterization of magnet/gradient systems, Magn. Reson. Med. 20 (1991) 268–284.

[2] S. Crozier, C.D. Eccles, F.A. Beckey, J. Fields, D.M. Doddrell, Correction of eddy-current-induced B0 shifts by receiver reference-phase modulation, J. Magn. Reson. 97 (1992) 661–665.

[3] P. Jehenson, M. Westphal, N. Schuff, Analytical method for the compensation of eddy-current effects induced by pulsed magnetic field gradients in NMR systems, J. Magn. Reson. 90 (1990) 264–278.

[4] G. Ries, Eddy current transients and forces in cryostat walls of superconducting solenoids, IEEE Trans. Magn. 24 (1988) 516–519.

[5] C. Boesch, R. Gruetter, E. Martin, Temporal and spatial analysis of fields generated by eddy currents in superconducting magnets: optimization of corrections and quantitative characterization of magnet/gradient systems, Magn. Reson. Med. 20 (1991) 268–284.

[6] T. Takahashi, Numerical analysis of eddy current problems involving z gradient coils in superconducting MRI magnets, IEEE Trans. Magn. 26 (1990) 893–896.

[7] T. Takahashi, Numerical analysis of Eddy current problems involving saddle-shaped coils in superconducting MRI magnets, IEEE Trans. Magn. 27 (1991) 3996–3999.

[8] W.A. Edelstein, T.K. Kidane, V. Taracila, T.N. Baig, T.P. Eagan, Y.-C.N. Cheng, R.W. Brown, J.A. Mallick, Active-passive gradient shielding for MRI acoustic noise reduction, Magn. Reson. Med. 53 (2005) 1013–1017.

[9] P. Mansfield, B. Chapman, Active magnetic screening of gradient coils in NMR imaging, J. Magn. Reson. 66 (1986) 573–576.

[10] R. Turner, R.M. Bowley, Passive screening of switched magnetic field gradients, J. Phys. E Sci. Instrum. 19 (1986) 876–879.

[11] H. Sanchez-Lopez, M. Poole, S. Crozier, Evaluating passively shielded gradient coil configurations for optimal eddy current compensation, J. Phys. D: Appl. Phys. 43 (2010) 1–12.

[12] T.K. Kidane, W.A. Edelstein, T.P. Eagan, V. Taracila, T.N. Baig, Y.-C.N. Cheng, R.W. Brown, Active-passive shielding for MRI acoustic noise reduction: network analysis, IEEE Trans. Magn. 42 (2006) 3854–3860.

[13] F. Liu, S. Crozier, An FDTD model for calculation of gradient-induced eddy currents in MRI system, IEEE Trans. Appl. Supercond. 14 (2004) 1983–1989.

[14] A. Trakic, H. Wang, F. Liu, H. Sánchez-López, S. Crozier, Analysis of transient eddy currents in MRI using a cylindrical FDTD method, IEEE Trans. Appl. Supercond. 16 (2006) 1924–1936.

[15] Y. Chen, R. Mittra, P. Harms, Finite-difference time-domain algorithm for solving Maxwell's equations in rotationally symmetric geometries, IEEE Trans. Microwave Theory Tech. 44 (1996) 832–839.

[16] A. Canova, G. Gruosso, M. Repetto, Integral methods for analysis and design of low-frequency conductive shields, IEEE Trans. Magn. 39 (2003) 2009–2017.

[17] W.M. Frix, G.G. Karady, A circuital approach to estimate the magnetic field reduction of nonferrous metal shields, IEEE Trans. Magn. 39 (1997) 24–32.

[18] R. Turner, Gradient coil design: a review of methods, Magn. Reson. Imag. 11 (1993) 903–920.

[19] G.N. Peeren, Stream function approach for determining optimal surface currents, J. Comput. Phys. 191 (2003) 305–321.

[20] M.A. Brideson, L.K. Forbes, S. Crozier, Determining complicated winding patterns for shim coils using stream functions and the target-field method, Concepts Magn. Reson. 14 (2002) 9–18.

[21] J.R. Bowler, T.P. Theodoulidis, Eddy currents induced in a conducting rod of finite length by a coaxial encircling coil, J. Phys. D: Appl. Phys. 38 (2005) 2861–2868.

[22] R. Grimberg, E. Radu, O. Mihalache, A. Savin, Calculation of the induced electromagnetic field created by an arbitrary current distribution located outside a conductive cylinder, J. Phys. D: Appl. Phys. 30 2285 30 (1997) 2285–2291.

[23] J.W. Carlson, K.A. Derby, K.C. Haveryszko, M. Weideman, Design and evaluation of shielded gradient coils, Magn. Reson. Med. 26 (1992) 191–206.

[24] S. Crozier, C.D. Eccles, F.A. Beckey, J. Fields, D.M. Doddrell, Correction of eddy-current-induced B0 shifts by receiver reference-phase modulation, J. Magn. Reson. 97 (1992) 661–665.

[25] E.E. Kriezis, T.D. Tsiboukis, S.M. Panas, J.A. Tegopoulos, Eddy currents: theory and application, Proceedings of the IEEE 80 (1992) 1559–1589.

[26] R. Bowtell, P. Robyr, Multilayer gradient coil design, J. Magn. Reson. 131 (1998) 286–294.

[27] J. Leggett, S. Crozier, S. Blackband, B. Beck, R.W. Bowtell, Multilayer transverse gradient coil design, Concepts Magn. Reson. Part B (Magn. Reson. Eng.) 16B (2003) 38–46.

[28] S. Crozier, W.U. Roffmann, K. Luescher, C. Snape-Jenkinson, L.K. Forbes, D.M. Doddrell, An openable high-strength gradient set for orthopedic MRI, J. Magn. Reson. 139 (1999) 81–89.

[29] H. Sanchez-Lopez, M. Poole, S. Crozier, An improved equivalent magnetization current method applied to the design of local breast gradient coils, J. Magn. Reson. 199 (2009) 48–55.

[30] R. Lemdiasov, R. Ludwig, M. Brevard, C. Ferris, Design and implementation of a uniplanar gradient field coil for magnetic resonance imaging, Concepts Magn. Reson. 20B (2004) 17–29.

[31] Peter T. While, L.K. Forbes, S. Crozier, 3D Gradient coil design – toroidal surfaces, J Magn Reson 198 (2009) 31–40.

[32] J. Herbert, P. Neff, Introductory Electromagnetics, John Wiley & Sons, Inc., Canada, 1991.

[33] MATLAB®, 2007. <www.mathworks.com>.

[34] K.R. Davey, On the use of the eigenvalue approach in the prediction of transient eddy current fields, IEEE Trans. Magn. 24 (1998) 190–192.

[35] W. Peterson, The fixed point method approach to nonlinear open boundary eddy current problems under TM field excitation, Electr. Eng. 78 (1995) 159–164.

[36] A. Trakic, F. Liu, H. Sanchez Lopez, H. Wang, S. Crozier, Longitudinal gradient coil optimization in the presence of transient eddy currents, Magn. Reson. Med. 57 (2007) 1119–1130.

[37] H. Wang, A. Trakic, L. Xia, F. Liu, S. Crozier, An MRI-dedicated parallel FDTD scheme, Concepts Magn. Reson. Part B (Magn. Reson. Eng.) 31B (2007) 147–161.